Molecular Biology of the Cell
Vol. 21, 1546–1555, May 1, 2010

Phosphatidylinositol 4,5-bisphosphate Directs Spermatid Cell Polarity and Exocyst Localization in *Drosophila*

Lacramioara Fabian,*† Ho-Chun Wei,*† Janet Rollins,‡ Tatsuhiko Noguchi,§ J. Todd Blankenship,‖ Kishan Bellamkonda,*¶ Gordon Polevoy,* Louis Gervais,# Antoine Guichet,# Margaret T. Fuller,@ and Julie A. Brill*¶

*Program in Developmental and Stem Cell Biology, The Hospital for Sick Children, Toronto, ON M5G 1L7, Canada; ‡Division of Natural Science, The College of Mount Saint Vincent, Riverdale, NY 10471; §Laboratory for Morphogenetic Signaling, RIKEN Center for Developmental Biology, Kobe, Hyogo 650-0047, Japan; ‖Department of Biological Sciences, University of Denver, Denver, CO 80208; ¶Department of Molecular Genetics, University of Toronto, Toronto, ON M5S 1A8, Canada; #Institut Jacques Monod, CNRS-University of Paris Diderot, 75205 Paris, France; and @Department of Developmental Biology, Stanford University School of Medicine, Palo Alto, CA 95305

Submitted July 17, 2009; Revised February 18, 2010; Accepted March 5, 2010
Monitoring Editor: Marcos Gonzalez-Gaitan

During spermiogenesis, *Drosophila melanogaster* spermatids coordinate their elongation in interconnected cysts that become highly polarized, with nuclei localizing to one end and sperm tail growth occurring at the other. Remarkably little is known about the signals that drive spermatid polarity and elongation. Here we identify phosphoinositides as critical regulators of these processes. Reduction of plasma membrane phosphatidylinositol 4,5-bisphosphate (PIP_2) by low-level expression of the PIP_2 phosphatase SigD or mutation of the PIP_2 biosynthetic enzyme Skittles (Sktl) results in dramatic defects in spermatid cysts, which become bipolar and fail to fully elongate. Defects in polarity are evident from the earliest stages of elongation, indicating that phosphoinositides are required for establishment of polarity. Sktl and PIP_2 localize to the growing end of the cysts together with the exocyst complex. Strikingly, the exocyst becomes completely delocalized when PIP_2 levels are reduced, and overexpression of Sktl restores exocyst localization and spermatid cyst polarity. Moreover, the exocyst is required for polarity, as partial loss of function of the exocyst subunit Sec8 results in bipolar cysts. Our data are consistent with a mechanism in which localized synthesis of PIP_2 recruits the exocyst to promote targeted membrane delivery and polarization of the elongating cysts.

INTRODUCTION

Cell polarity is a prerequisite for differentiation, proliferation and morphogenesis in all organisms. The activity and localization of the cytoskeleton, polarity complexes, signaling networks, and membrane trafficking associated with polarization are regulated by the lipid composition of organelles and membrane domains, in particular by phosphorylated derivatives of phosphatidylinositol (PI), also called phosphoinositides, which function as spatially restricted molecular signals (Odorizzi *et al.*, 2000; Behnia and Munro, 2005; Di Paolo and De Camilli, 2006). Phosphoinositides are membrane-tethered lipid molecules synthesized from PI by the sequential action of lipid kinases (Figure 1A). Local concentrations of particular phosphoinositides are controlled by the subcellular localization or activation of lipid kinases, lipases, and phosphatases (Roth, 2004). For example, plasma membrane PI 4,5-bisphosphate (PIP_2) is synthesized from PI 4-phosphate (PI4P) by PI4P 5-kinases (PIP5Ks) and can in turn be phosphorylated by PI 3-kinases (PI3Ks) to yield PI 3,4,5-trisphosphate (PIP_3). PIP_2 can also be hydrolyzed by phospholipase C (PLC) to produce the second messengers inositol trisphosphate (IP_3) and diacylglycerol (DAG) or dephosphorylated by phosphoinositide phosphatases to regenerate PI4P. Importantly, in addition to serving as a precursor for other signaling molecules, PIP_2 itself is thought to act as a potent membrane signal (Di Paolo and De Camilli, 2006).

PIP_2 regulates diverse targets, including actin regulators and membrane-trafficking proteins (Takenawa and Itoh, 2001; Yin and Janmey, 2003; De Matteis and Godi, 2004; Behnia and Munro, 2005; Niggli, 2005; Balla, 2006; Oude Weernink *et al.*, 2007). High levels of PIP_2 promote filamentous (F) actin assembly by directly binding and regulating proteins that control actin polymerization (Yin and Janmey, 2003). PIP_2 links F-actin to the plasma membrane via membrane-cytoskeleton cross-linkers such as spectrin and moesin (Niggli *et al.*, 1995; Hirao *et al.*, 1996). Subunits of the exocyst—a conserved octameric protein complex that directs localized membrane addition—contain basic regions that interact with PIP_2 (He *et al.*, 2007; Liu *et al.*, 2007; Zhang *et al.*, 2008; Yamashita *et al.*, 2010). The exocyst directs membrane trafficking events required for cell polarization and growth during development in plants and animals and was recently shown to be required for ciliary membrane formation in Madin-Darby canine kidney (MDCK) cells (Hsu *et al.*, 2004; Somers and Chia, 2005; Hala *et al.*, 2008; Zuo *et al.*, 2009). However, the role of PIP_2 binding in exocyst function during development of a complex multicellular organism remains unknown.

This article was published online ahead of print in *MBoC in Press* (http://www.molbiolcell.org/cgi/doi/10.1091/mbc.E09–07–0582) on March 17, 2010.

† Co-first authors who contributed equally to this work.

Address correspondence to: Julie A. Brill (julie.brill@sickkids.ca).

To study the role of phosphoinositides in cell polarity, we are using *Drosophila* sperm development as a model system. Spermatogenesis in *Drosophila* initiates by division of a germline stem cell to form a gonial cell, which then divides four times to produce a group of 16 primary spermatocytes. The spermatocytes grow in size and undergo meiosis to generate a group of 64 haploid spermatids. Because germ cell cytokinesis is incomplete, groups of cells remain connected through stable intercellular bridges called ring canals and develop within a syncytial cytoplasm or cyst. Male germline ring canals contain the actin-associated protein anillin and associate with the fusome, a spectrin-rich membranous organelle that interconnects the developing germ cells and localizes to the growing end of the sperm tails in a honeycomb structure (Hime *et al.*, 1996).

Drosophila spermatids undergo dramatic changes in shape as they develop from small round cells ~12 μm in diameter to elongated cells nearly 1.8 mm in length (Figure 1B; Tates, 1971; Tokuyasu, 1975). In early round spermatids, the basal body forms a stable attachment to the nuclear envelope (Figure 1Bi). The microtubule-based flagellar axoneme grows out from the basal body, and two mitochondrial derivatives elongate along the length of the axoneme (Figure 1B, i–iii). The distal (growing) end of the elongating axoneme is covered by a flagellar membrane—topologically equivalent to a ciliary membrane—that remains contiguous with the plasma membrane throughout axoneme assembly (Figure 1Biv; Fritz-Niggli and Suda, 1972; Tokuyasu, 1975). During elongation, each cyst becomes highly polarized, with nuclei localizing to one end and the fusome and ring canals localizing to the growing end (Hime *et al.*, 1996; Ghosh-Roy *et al.*, 2004). Spermatid elongation and individualization of mature sperm require a substantial increase in cell surface area. Hence, membrane addition is a critical aspect of sperm maturation.

Here, we show that polarized organization of elongating spermatids within cysts depends on normal levels of PIP_2. When PIP_2 levels are reduced, nuclei localize to both ends of the cysts and sperm tails grow toward the middle. The exocyst, which normally colocalizes with PIP_2 at the growing end, is uniformly distributed when PIP_2 levels are reduced, suggesting a defect in targeted membrane delivery. We demonstrate that both the PIP5K Sktl and the exocyst are required for normal polarization and elongation of spermatid cysts. Our results suggest that local synthesis of PIP_2 plays a critical role in establishing cyst polarity by recruiting the exocyst complex to drive spermatid cell growth.

MATERIALS AND METHODS

Fly Stocks

Flies were raised and maintained on standard cornmeal molasses agar at 25°C. Transgenic flies were generated by injection of w^{1118} embryos with constructs derived from the testis vector tv3, which contains the spermatocyte-specific β_2-tubulin promoter (Hoyle and Raff, 1990; Wong *et al.*, 2005; Wei *et al.*, 2008). Lines expressing PLCδ-PH-green fluorescent protein (GFP) and PLCδ-PH-red fluorescent protein (RFP; which bind plasma membrane PIP_2; Lemmon *et al.*, 1995; Varnai and Balla, 1998), RFP-PH-FAPP (which binds PI4P; Dowler *et al.*, 2000), yellow fluorescent protein-Skittles (YFP-Sktl) and SigD-high (R19) were described previously (Wong *et al.*, 2005; Wei *et al.*, 2008). Two transgenic lines (R1 and R7) mapped to the X chromosome and expressed lower levels of SigD, a phenomenon commonly observed for expression of X-linked transgenes in developing male germ cells (Hense *et al.*, 2007; our unpublished observations). Although R1 was used for all experiments shown, similar results were obtained with R7. Because R1 and R7 are dominant male-sterile, fertile stocks were established using the X chromosome balancer FM7i, which carries a *white* mutant allele (w^1) to allow for selection of the w^+ SigD transgene. Exocyst mutants were identified in screens for viable but male sterile mutants (Giansanti *et al.*, 2004; Wakimoto *et al.*, 2004). The *onion rings* (*onr*; Exo84) allele contains a nonsense mutation that is predicted to produce a truncated protein of 581 rather than 672 amino acids (Blankenship *et al.*, 2007). Evidence that *funnel cakes* (*fun*) encodes *Drosophila* Sec8 will be presented elsewhere (J. T. Blankenship, M. Giansanti, C. Robinett, M. Gatti, and M. T. Fuller, unpublished data). Both mutants were examined *in trans* to deficiencies that uncover the corresponding genes (*Df(3R)Espl3* in the case of *onr* and *Df(3R)Exel6145* in the case of *fun*). β-Tubulin-GFP (Inoue *et al.*, 2004) flies were a gift from Yasuko Akiyama-Oda and Hiroki Oda (JT Biohistory Research Hall, Osaka, Japan). Unc-GFP (Baker *et al.*, 2004) flies were generously provided by James Baker and Maurice Kernan (SUNY Stony Brook, Stony Brook, NY). $sktl^{2.3}$ is a hypomorphic allele of *sktl* that affects polarity during *Drosophila* oogenesis (Gervais *et al.*, 2008). Clones of germ cells mutant for $sktl^{2.3}$ were generated in flies of genotype *w*, hsFLP/Y; FRT42B, $sktl^{2.3}$/FRT42B, and Ubi-GFP.nls using the FLP-FRT (fragment length polymorphism and recognition target system, respectively; Golic and Lindquist, 1989). hs-FLP and FRT42B, Ubi-GFP.nls stocks were obtained from the Bloomington *Drosophila* Stock Center (Bloomington, IN). Complete genotypes of fly stocks are available upon request.

Fluorescence Microscopy

For live preparations of *Drosophila* male germ cells, testes from newly eclosed males were dissected in testis isolation buffer (Casal *et al.*, 1990) containing 8.3 μg/ml Hoechst 33342 (Sigma-Aldrich, St. Louis, MO) to stain DNA and squashed under a coverslip, as previously described (Wei *et al.*, 2008).

Spermatid cyst length was determined from phase-contrast micrographs of fixed preparations obtained from 1-d-old adult males. Germ cells were stained for F-actin and DNA (see below) to mark the ends of the cysts and to determine the stage of cyst elongation. Full-length wild-type cysts were identified by the presence of actin-containing investment cones. SigD-low cysts were measured at the latest identified stages, based on the shape and distribution of the nuclei. Because cysts were often bent, segmental measurements were obtained using Axiovision software (Carl Zeiss, Oberkochen, Germany) and then summed to determine the total length. Average length and SD were calculated using Microsoft Excel (Microsoft, Redmond, WA).

Sample preparation for fluorescent staining was performed as described (Wei *et al.*, 2008). Primary antibodies were used at the following concentrations: 1:250 mouse IgM anti-PIP_2 (Echelon Biosciences, Logan, UT); 1:500 guinea pig anti-Sec8 and 1:1000 guinea pig anti-Sec6 (gifts from Slobodon Beronja and Ulrich Tepass [University of Toronto, Toronto, Canada]; Beronja *et al.*, 2005); 1:1000 mouse anti-acetylated α-tubulin 6-11-B (Sigma-Aldrich); 1:500 rabbit anti-phospho-moesin (P-moesin; gift from Sebastien Carreno [Institute for Research in Immunology and Cancer, Montreal, Canada]; Carreno *et al.*, 2008); 1:100 rabbit anti-anillin (from Christine Field [Harvard Medical School, Boston, MA] or from our lab; Field and Alberts, 1995; Goldbach *et al.*, 2010); 1:500 mouse anti-α-spectrin (Developmental Studies Hybridoma Bank, Iowa City, IA); 1:1000 rabbit anti-centrosomin (Cnn; gift from Thomas Kaufman [Indiana University, Bloomington, IN]; Li *et al.*, 1998) 1:500 mouse anti-GFP 3E6 (Molecular Probes, Eugene, OR). F-Actin was stained with 1 U/ml rhodamine phalloidin or Alexa 488 phalloidin, as recommended by the manufacturer (Molecular Probes). Secondary antibodies were conjugated to Alexa fluorochromes (Molecular Probes) and were used at 1:1000. DAPI (5 μg/ml; Molecular Probes) was used to stain DNA.

Preparations were examined on an upright Zeiss Axioplan 2 epifluorescence microscope equipped with an Axiocam black and white camera using Axiovision software (Carl Zeiss). Confocal images were obtained on an inverted Zeiss spinning disk confocal microscope with Volocity software (Improvision, PerkinElmer, Waltham, MA) or on an inverted Zeiss LSM510 laser-scanning confocal microscope using LSM Image software (The Hospital for Sick Children Imaging Facility). Unless indicated, groups of images were obtained using the same conditions (light intensity, exposure time) and were adjusted in an identical manner for brightness, contrast and pseudocolor with Adobe Photoshop (Adobe Systems, San Jose, CA).

Immunoblotting

Samples for immunoblotting were prepared using 20 pairs of testes per lane for each genotype. Testes from newly eclosed males were dissected in testis isolation buffer and boiled for 5 min in Laemmli sample buffer (Sambrook *et al.*, 1989). Proteins were separated in a 10% SDS-polyacrylamide gel and transferred to a nitrocellulose membrane (Amersham, GE Healthcare, Little Chalfont, Buckinghamshire, United Kingdom) using a Trans-Blot SemiDry transfer apparatus (Bio-Rad, Mississauga, ON, Canada). Blots were probed sequentially with rabbit anti-SigD (gift of Brett Finlay, University of British Columbia, Vancouver, Canada, and John Brumell, The Hospital for Sick Children, Toronto, Canada) and mouse anti-acetylated α-tubulin (6-11-B, Sigma-Aldrich) antibodies, which were used at 1:1000 and 1:5000, respectively. HRP-conjugated anti-rabbit and anti-mouse secondary antibodies (Amersham) were diluted 1:10,000 and visualized using chemiluminescence (ECL Plus kit, Amersham).

Electron Microscopy

Testis samples for transmission electron microscopy (TEM) were prepared as described (Bazinet and Rollins, 2003; Wei *et al.*, 2008). Samples for immuno-electron microscopy were prepared using a protocol modified from Peters *et al.* (2006). Briefly, *Drosophila* testes were dissected in phosphate buffer, pH 7.4, placed immediately in 4% paraformaldehyde, and fixed overnight at 4°C. The samples were rinsed twice with 1.5 M glycine in phosphate-buffered saline (PBS) for 5 min and then taken through serial dilutions of 1, 5, and 12% gelatin (Electron Microscopy Sciences, Hatfield, PA), for 10 min each. Testes were

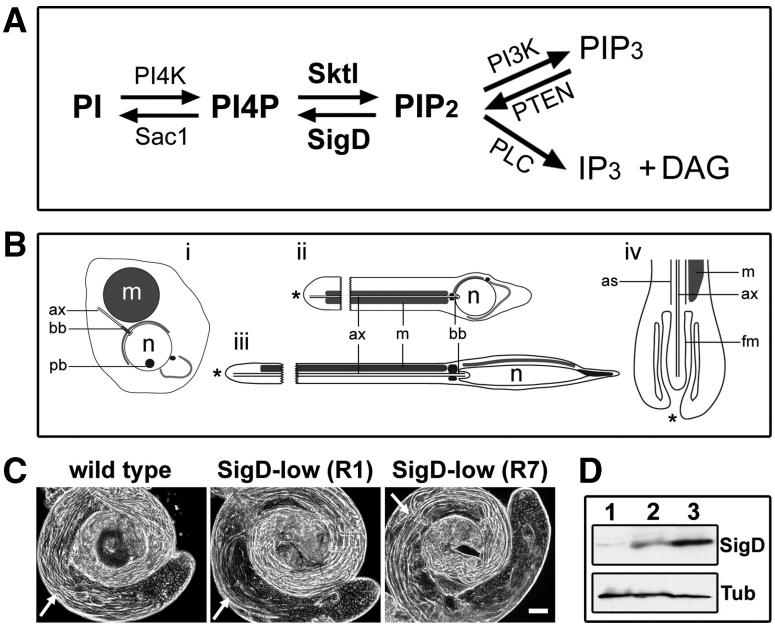

Figure 1. Expression of low levels of SigD in *Drosophila* testes causes mild defects in sperm development. (A) Phosphatidylinositol (PI) pathway. PI can be phosphorylated by PI 4-kinases (PI4K) to yield PI4P and then by PIP 5-kinases (PIP5K) such as *Drosophila* Sktl, to produce PIP_2. PIP_2 can be further phosphorylated by PI 3-kinase to generate PIP_3, which in turn can be dephosphorylated by PTEN phosphatase to regenerate PIP_2. PIP_2 can also be hydrolyzed by phospholipase C (PLC), to generate second messengers inositol trisphosphate (IP_3) and diacylglycerol (DAG), or sequentially dephosphorylated by 5-phosphatases, including *Salmonella* SigD, to regenerate PI4P, which in turn can be dephosphorylated by 4-phosphatases such as *Drosophila* Sac1, to produce PI. (B) Schematic representation of spermatid elongation in *Drosophila* (adapted from Tates, 1971; Tokuyasu, 1975). (i) Early round spermatid. (ii) Mid-elongated spermatid. (iii) Late elongated spermatid. (iv) Detail of the growing end of a spermatid. Growing ends are indicated by asterisks (ii–iv). m, mitochondrial derivative; n, nucleus; ax, axoneme; bb, basal body; pb, protein body; as, axial sheath; fm, flagellar membrane. (C) Phase-contrast images of live whole-mount *Drosophila* testes showing normal morphology in wild type and superficially normal morphology in two SigD-low lines (R1 and R7). Arrows indicate elongated spermatid cysts. Scale bar, 10 μm. (D) SigD expression in *Drosophila* testes. Immunoblot of testis protein extracts probed with antibodies to SigD and acetylated α-tubulin (Tub) as a loading control. Lane 1, wild type; lane 2, SigD-low (R1); lane 3, SigD-high (R19). R1 expresses lower levels of SigD protein than R19.

transferred to a warm Chang mold for flat embedding (Electron Microscopy Sciences) and covered with warm 12% gelatin. Molds were placed at 4°C for 30 min. Regions of interest were excised from the gelatin blocks, transferred to vials with PBS (without Ca^{2+} and Mg^{2+}) for 10 min, and then placed in a 2.3 M sucrose solution in PBS (without Ca^{2+} and Mg^{2+}) overnight at 4°C. Individual testes were cut from the gelatin blocks, transferred to color-marked pins, and then immersed in liquid nitrogen. Pins were stored in liquid nitrogen before sectioning with a Leica Ultracut UCT microtome with an FCS cryochamber (Leica Microsystems, Wetzlar, Germany). Cryosections (80 nm thick) were blocked for 30 min with 5% cold water fish gelatin, incubated with 1:100 rabbit anti-GFP for 30 min, rinsed five times for 2 min with PBS, incubated with 6-nm gold-conjugated secondary antibodies (Electron Microscopy Sciences) for 30 min, rinsed five times for 2 min with PBS, fixed 10 min with 2.5% glutaraldehyde, rinsed two times for 2 min with PBS followed by five times for 2 min with distilled water, and finally stained for 10 min with 2% methylcellulose and 0.4% uranylacetate.

Sections were viewed with a JEOL JEM 1200EX TEM, a JEOL JTE 141011 (JEOL, Peabody, MA; The Hospital for Sick Children Electron Microscopy Facility), or a Tecnai TEM (Tecnai, Hillsboro, OR; Advanced Bioimaging Centre at The Hospital for Sick Children and Mt. Sinai Hospital). Images were obtained using AMTv542 (Advanced Microscopy Techniques, Danvers, MA) and Gatan Digital Micrograph (Gatan, Pleasanton, CA) acquisition software and were manipulated only for brightness and contrast using Adobe Photoshop.

In Vitro Culture of Elongating Spermatids

Isolated cysts of *Drosophila* spermatids were cultured as described (Noguchi and Miller, 2003). Briefly, testes from newly eclosed wild-type or SigD-low adult males were dissected and transferred into MM3 culture media containing 10% fetal calf serum (Sigma-Aldrich) and standard penicillin/streptomycin cocktail. Time-lapse differential interference contrast (DIC) videos were recorded from onion stage to early elongation stages. Elongation was recorded using a DeltaVision system (Applied Precision, Issaquah, WA) on a IX70 (Olympus, Tokyo, Japan) microscope equipped with 40×S UplanApo objective (Olympus). QuickTime videos (10 fps) were created by ImageJ (http://rsb.info.nih.gov/ij/) and compressed by MPEG-4.

RESULTS

Reduction of Plasma Membrane PIP_2 Causes Male Sterility

During experiments to test the roles of phosphoinositides during *Drosophila* sperm development, we generated lines of transgenic flies expressing the *Salmonella* PIP_2 phosphatase SigD (also called SopB) under control of the spermatocyte-specific β_2-tubulin promoter (see *Materials and Methods*). Two of the SigD-expressing lines (denoted R1 and R7) had superficially normal testes that contained elongated spermatid cysts (Figure 1C). R1 and R7, unlike the other SigD-expressing lines with severe phenotypes, carried transgenes on the X chromosome and expressed lower levels of SigD (Figure 1D; R7, not shown). We refer to these lines as SigD-low to distinguish them from the previously described lines, which we call SigD-high. Because R1 and R7 behaved identically, for the purposes of this study we focused on R1.

Expression of low levels of SigD caused a significant reduction in plasma membrane PIP_2, as visualized by localization of fluorescent markers that specifically bind PIP_2. In wild-type spermatocytes, early spermatids and elongating spermatids (Figure 2, A′ and D′), PLCδ-PH-GFP, a green fluorescent marker that specifically binds PIP_2, was mainly associated with the plasma membrane, whereas in SigD-low, PLCδ-PH-GFP was cytoplasmic, with low or undetectable levels on the plasma membrane (Figure 2, B′ and E′). There was no obvious difference in the distribution of RFP-PH-FAPP, a red fluorescent PI4P-binding protein, in SigD-low versus wild-type cells, suggesting that levels of PI4P were not significantly affected (not shown). However, we cannot rule out a subtle increase in PI4P below the level of detection with the fluorescent marker. Overexpression of the PIP5K Skittles (Sktl)—which synthesizes PIP_2 from PI4P—suppressed loss of plasma membrane PIP_2 in the context of SigD-low; PLCδ-PH-RFP was restored to the plasma membrane in spermatocytes and early spermatids (Figure 2C′) and partially restored in elongated spermatids (Figure 2F′).

PIP_2 Is Required for Spermatid Cyst Polarity and Elongation

Analysis of the morphology of developing germ cells in SigD-low males revealed defects in spermatid cyst elongation and polarity. Wild-type cysts of elongating spermatids were 1.75 ± 0.19 mm long (n = 17) and unipolar, with nuclei clustered at one end of the cyst (Figure 3, A, E, I, M, and O).

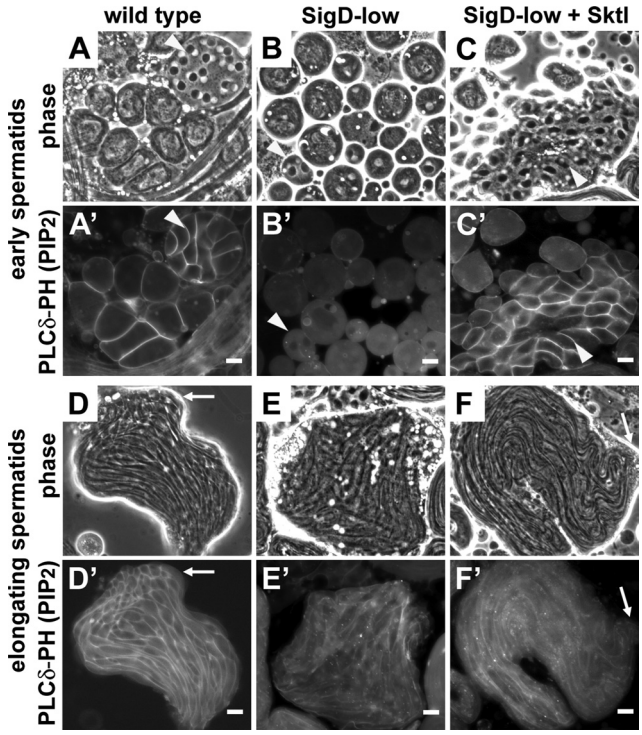

Figure 2. Low levels of SigD reduce plasma membrane PIP$_2$. (A–F) Phase-contrast (phase) and (A′–F′) corresponding fluorescence images of live squashed preparations of male germ cells expressing PLCδ-PH-GFP (A′, B′, D′, and E′) or -RFP (C′ and F′), which bind PIP$_2$. Arrowheads, early round spermatids; arrows, growing ends of spermatid cysts. SigD-low cysts lack a growing end (see text). PIP$_2$ is found at the plasma membrane of wild-type early round spermatids (A′) and elongating spermatids (D′). Low levels of SigD reduce PIP$_2$ at the plasma membrane (B′) and cause accumulation of PLCδ-PH-GFP in the cytoplasm (B′ and E′). Coexpression of Sktl with SigD-low partially restores plasma membrane PIP$_2$ in early (arrowhead, C′) and elongating (F′) spermatids. Scale bars, 10 μm.

In contrast, early elongating cysts from SigD-low males showed scattered nuclei (Figure 3N) and later stage SigD-low cysts were much shorter than wild-type cysts of comparable stage (0.91 $\pm$ 0.09 mm long; n = 24) and appeared bipolar, with nuclei distributed between the two ends (Figure 3, B and F) and sperm tails growing toward the middle of the cyst (Figure 3, B, F, J, and P). Bipolarity of SigD-low cysts was partially rescued by coexpression of Sktl (Figure 3, C, G, and K). Suppression of SigD-low by Sktl overexpression strongly suggested that spermatid cyst polarity relies on PIP$_2$ or on the correct balance between PIP$_2$ and PI4P (see *Discussion*). Note that for simplicity we will henceforth refer to this as a requirement for PIP$_2$.

Endogenous Sktl is required for spermatid cyst polarity, as revealed by analysis of marked clones of male germ cells homozygous mutant for *sktl*$^{2.3}$ (see *Materials and Methods*). *sktl* mutant cysts exhibited striking defects in polarity, similar to those observed in SigD-low (Figure 3, D and H), and mild cytokinesis defects (not shown), similar to those previously observed in SigD-high, suggesting that PIP$_2$ levels are critically important for multiple aspects of male germ cell development. In addition, this result validates the use of SigD-low as a tool to study the role of PIP$_2$ in spermiogenesis.

The polarized distribution of F-actin and the actin-associated proteins spectrin, anillin, and moesin was dependent on PIP$_2$ levels. As previously reported, spectrin showed a polarized localization to the fusome in early stages of elongation (not shown) and, in later stages, to a honeycomb-like structure along the membranes at the growing end of wild-type cysts (Figure 3, I and L). In SigD-low cysts, the honeycomb structure failed to form and a fusome-like spectrin structure was observed in the middle of the bipolar cysts (Figure 3J). The polarized distribution of spectrin was largely restored by coexpression of Sktl (Figure 3K). In wild-type cysts, the highest concentration of actin filaments was found at the growing end (Figure 3, M and O), near the ring canals, which contain anillin (Figure 3M). P-moesin also localized to ring canals (Figure 3O). SigD-low cysts had fewer actin filaments, and these were fairly evenly distributed throughout the cysts (Figure 3, N and P). Anillin and P-moesin remained associated with ring canals, but these were scattered at early stages of elongation (Figure 3N; P-moesin, not shown) and relocalized to the middle of the bipolar cysts at later stages (Figure 3P; anillin, not shown).

PIP$_2$ Reduction Disrupts Polarity during Early Stages of Elongation

Proper levels of PIP$_2$ are required at the earliest stages of elongation to ensure correct polarized orientation of individual elongating spermatids, as revealed by real-time imaging of wild-type and SigD-low spermatids cultured on polylysine-coated glass dishes (Figure 4A). In these experiments, groups of interconnected spermatids remained attached by ring canals at the elongating end, which adhered to the dish. Thus, the nuclear ends of the individual spermatids appeared to grow outward, away from each cluster of cells. In wild-type spermatids, polarity was established early (Figure 4A, top panels and diagrams; see also Supplemental Video 1). Each nucleus-basal body pair became associated with one end of the elongating mitochondrial derivative, the nucleus appeared to form a tight association with the plasma membrane, and all sperm tails elongated in the same direction (Figure 4A, t = 05:26, red arrows). In SigD-low cysts, the relationship of the nucleus with the mitochondrial derivative was more fluid (Figure 4A, bottom panels and diagrams; see also Supplemental Video 2). The nucleus-basal body pair appeared to move freely along the length of the early elongating spermatid, the nucleus failed to associate tightly with the plasma membrane, and different spermatids within a group elongated in different directions (Figure 4A, 5 = 07:02, red arrows).

Basal Body Orientation Requires PIP$_2$

Normal levels of PIP$_2$ are required for basal body docking and for proper orientation of the nucleus and basal body with respect to the direction of growth of the spermatid cyst. Analysis of the basal body marker Unc-GFP and the centrosomal protein Cnn revealed that in wild-type spermatids Unc-GFP and Cnn were associated with a single basal body per nucleus (Figure 4, B and C). All nucleus-basal body pairs were oriented in the same direction, with the nuclei adjacent to the plasma membrane and basal bodies oriented away from the membrane (Figure 4, B and C, and inset in B). In SigD-low spermatids, Unc-GFP and Cnn were generally present at the expected position of the basal body (Figure 4, E and F), and most basal bodies were near a nucleus. However, nucleus-basal body pairs were oriented in different directions, with some of the basal bodies found next to the plasma membrane (Figure 4, E and F, and inset in E). Immunoelectron microscopy showed that Unc-GFP, which localized to the basal body in wild type (Figure 4D, inset), was properly localized in SigD-low, but its levels were reduced

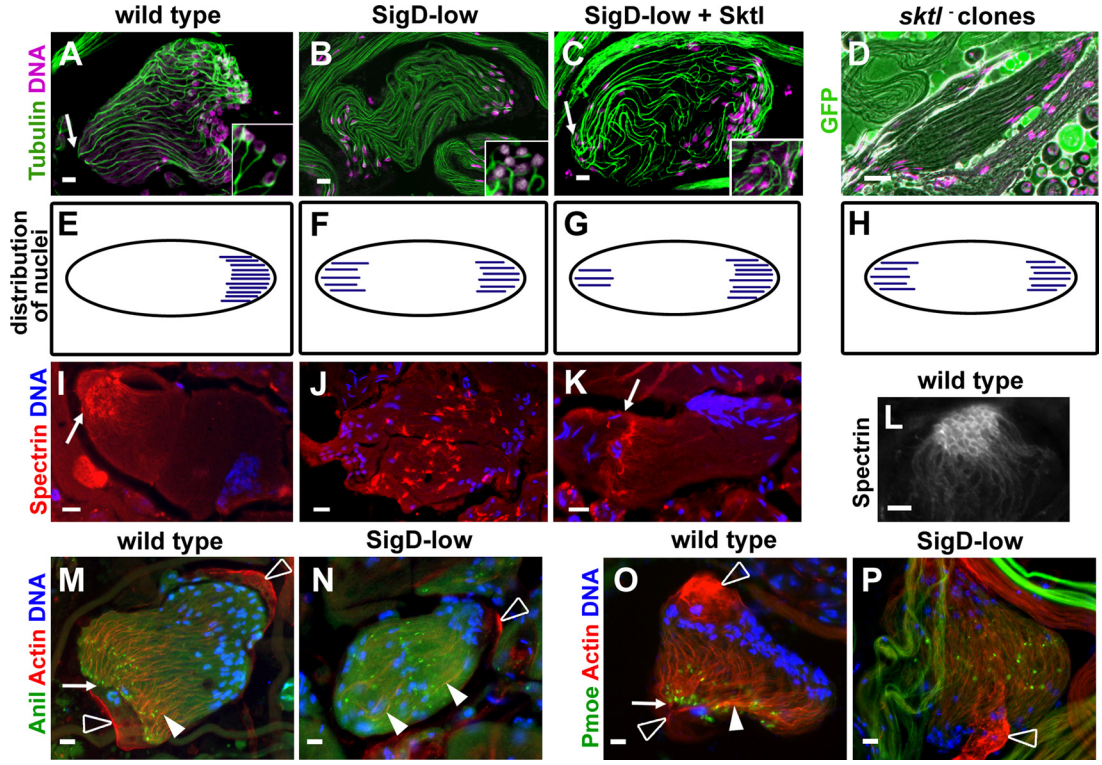

Figure 3. Normal levels of PIP_2 are required for spermatid cyst polarity and polarized distribution of F-actin and actin-associated proteins. Fluorescence micrographs of elongating spermatid cysts. Arrows, growing ends. (A–C) Confocal micrographs of elongated *Drosophila* cysts stained for DNA (magenta) and tubulin (green). (A) Wild-type cyst with nuclei at one end. (B) SigD-low bipolar cyst, with nuclei at both ends. (C) Coexpression of Sktl with SigD-low partially rescues cyst polarity. (Insets, A–C) Single confocal sections showing perinuclear microtubule arrays, which are disorganized in SigD-low. Tubulin was stained with antibodies directed against acetylated α-tubulin (A and C) or GFP (to visualize β-tubulin-GFP (B). (D) Epifluorescence micrograph of a live squashed preparation of male germ cells stained for DNA (magenta), showing a bipolar $sktl^{2.3}$ mutant clone (see *Materials and Methods*). Cysts mutant for $sktl^{2.3}$ are marked by the absence of GFP (green). (E–H) Diagrams illustrating the polarity of wild-type (E), SigD-low (F), partially rescued (SigD-low + Sktl; G) and $sktl^{-}$ (H) cysts. (I–K) Epifluorescence micrographs showing elongated spermatid cysts stained for α-spectrin (red) and DNA (blue). In wild type (I), spectrin localizes to the growing end of the elongating cyst. In SigD-low (J), spectrin localizes to the middle of the cyst. (K) Localization of spectrin is partially rescued by coexpression of Sktl with SigD-low. (L) Confocal image showing localization of α-spectrin in the honeycomb at the growing end of a wild-type cyst. (M–P) Epifluorescence micrographs of elongating cysts showing F-actin (red), DNA (blue), and anillin (Anil, green), and M and P-moesin (Pmoe, green; O and P). Colocalization (yellow). In wild type, anillin (M) and P-moesin (O) localize to ring canals near where F-actin is concentrated at the growing end (arrowheads, arrows). In SigD-low, anillin (N) and P-moesin (P) remain associated with ring canals, which are scattered (N) or which localize to the middle of the cyst (P). Actin filaments are distributed along the cyst (arrowheads, N). White open arrowheads, cyst cells. Scale bars (A–C and L–P), 10 μm; (D and I–K) 20 μm.

(Figure 4G, inset). In a few cases, basal bodies of apparently normal architecture were found in the absence of any obvious nuclear envelope (Figure 4G), similar to what we had observed for SigD-high.

Sktl Localizes to the Growing End of Spermatid Cysts

Sktl becomes concentrated at the growing end of spermatid cysts, as determined by examining distribution of YFP-Sktl in wild-type spermatids. In early round spermatids, Sktl was evenly distributed along the plasma membrane (Figure 5A) and was concentrated at ring canals, where it colocalized with anillin (not shown). In early elongating spermatids, Sktl was found along the plasma membrane and the growing end (Figure 5C, arrow) on a linear structure of the expected length and morphology to be the flagellar membrane (Figure 5I, white arrowhead). By mid-elongation, Sktl was enriched in punctate and elongated structures (Figure 5, E and J, white arrowhead), many of which localized near ring canals at the growing end (Figure 5, I″ and J″, arrowheads, and insets in I″ and J″). At later stages, Sktl became concentrated on membranes near the growing end (Figure 5G). In contrast, YFP-Sktl failed to strongly concentrate at the growing end in SigD-low spermatids (Figure 5, D, F, and H, arrows).

PIP_2 Colocalizes with and Recruits the Exocyst to the Growing End of Spermatid Cysts

The exocyst, like PIP_2 and Sktl, was concentrated along membranes at the growing end of spermatid cysts, as revealed by immunofluorescence using antibodies that specifically recognize the exocyst subunits Sec8 and Sec6. Although the exocyst was present in cytoplasmic puncta that showed no obvious asymmetry in early round and elongating spermatids (not shown), at later stages of elongation the exocyst exhibited a highly polarized distribution. Sec8 and Sec6 were found in a honeycomb-like structure at the growing end of the spermatid cysts (Figure 6, B, C, and F, and insets), with PIP_2 appearing to surround the exocyst patches (Figure 6, A and C). In SigD-low spermatids, the localization of Sec8 and Sec6 was dramatically affected, with the two proteins showing a diffuse distribution throughout the entire cyst (Figure 6, D and G, and inset in G). Localization of

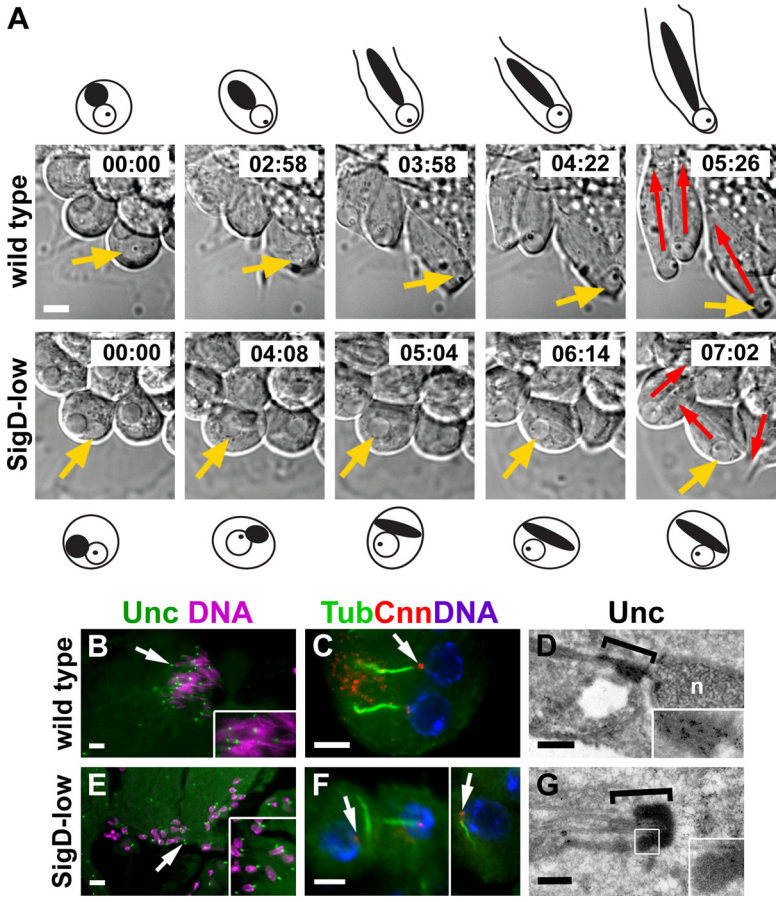

Figure 4. PIP_2 reduction disrupts spermatid polarity and basal body orientation during early stages of elongation. (A) DIC micrographs (still images) taken from time-lapse videos of wild-type (top) and SigD-low (bottom) spermatids cultured in vitro (see *Materials and Methods*). Yellow arrows show the location of the nucleus in the cell diagrammed above (wild type) or below (SigD-low) the still images. Mitochondrial derivatives (black circles and ovals) and nuclei (white circles) with protein bodies (black dots) are indicated in the diagrams. Red arrows show the direction of cell growth (away from the nucleus). Note that spermatids are roughly parallel in wild type, but their orientation is disturbed in SigD-low. Time is in hours:minutes. (B and E) Epifluorescence micrographs of live squashed preparations of elongating spermatids showing localization of the basal body marker Unc-GFP (green) relative to DNA (magenta). (C and F) Epifluorescence micrographs of fixed squashed preparations of elongating spermatids stained for the basal body marker Cnn (red), acetylated α-tubulin (Tub, green) and DNA (blue). In wild-type spermatids (B and C), Unc and Cnn associate with a single basal body per nucleus, with all nucleus–basal body pairs oriented in the same direction. In SigD-low spermatids (E and F), most basal bodies associate with a nucleus, but nucleus-basal body pairs are oriented in different directions. Insets, high-magnification views of nuclei and basal bodies. (D and G) Immunoelectron micrographs showing distribution of Unc-GFP at the basal body (brackets). The basal body in wild type (D) is embedded in the nuclear envelope (n, nucleus). The structure of basal body in SigD-low (G) appears normal, but is not attached to a nucleus. Insets, high-magnification micrographs showing Unc-GFP at the basal body. Black dots are gold particles. White square in G represents the area magnified in the inset. Scale bars, (A, C, and F) 5 μm; (B and E) 20 μm; (D and G) 500 nm.

Sec8 and PIP_2 to the growing end was largely restored by coexpression of Sktl with SigD-low (Figure 6, E and H), suggesting that PIP_2 recruits the exocyst to membranes near the sites of flagellar axoneme assembly and membrane addition.

The Exocyst Is Required for Spermatid Cyst Polarity during Elongation

Loss-of-function mutations in genes encoding exocyst subunits cause defects in spermatid cyst elongation and polarity reminiscent of the defects caused by forced expression of SigD. The *onr* gene encodes the *Drosophila* homolog of Exo84, and the *fun* gene encodes *Drosophila* Sec8. Testes from *onr*/Df flies revealed severe defects in spermatid elongation, with round cysts (Figure 7A) that completely lacked polarity (Figure 7, C and E), similar to the phenotype of SigD-high spermatids. Testes from *fun*/Df flies showed milder defects in spermatid elongation (Figure 7B) and had bipolar cysts (Figure 7, D and F), similar to the phenotype of SigD-low (Figure 3B). Consistent with *fun* being a partial loss-of-function allele, mutant testes showed reduced Sec8 staining, with no accumulation at the growing end of the cysts (Figure 7G). Sec6 was delocalized, but its levels were not visibly reduced in *fun*/Df testes (Figure 7H). The cytoskeletal proteins actin, anillin and spectrin did not redistribute to the middle of the bipolar cysts, but accumulated at the growing end of the cysts in *fun*/Df testes (Figure 7, I and J), in contrast to the mislocalization to the middle of the cysts observed in SigD-low testes. This difference raised the possibility that the defects in spermatid cyst polarity observed in exocyst mutants might be due to a primary defect in localized membrane trafficking rather than to secondary effects on cytoskeletal proteins. Ultrastructural analysis by TEM confirmed that both SigD-low and *fun* spermatid cysts are indeed bipolar, with axonemes growing from opposite directions. Mature wild-type axonemes contain nine doublet and two central-pair microtubules and are decorated with accessory microtubules and flagellar dyneins that confer rotational polarity to the axonemes. In wild-type cysts, all axonemes were oriented in the same direction (Figure 7K, curved red arrows), whereas axonemes in SigD-low or *fun* cysts were antiparallel (Figure 7, L and M, curved red arrows).

PIP_2 and the Exocyst Are Required for Plasma Membrane Addition during Spermatid Elongation

Ultrastructural analysis by TEM revealed defects in the plasma membrane in both SigD-low and *fun* spermatids, suggesting that reduction of PIP_2 by SigD-low and reduced function of Sec8 in *fun* mutants cause defects in membrane deposition during elongation. In wild type, each spermatid was surrounded by a plasma membrane that separated it from adjacent spermatids (Figure 7K). In contrast, the plasma membranes separating individual spermatids were largely absent in SigD-low and *fun*/Df spermatid cysts (Figure 7, L and M), indicating a defect in membrane addition during spermatid elongation.

DISCUSSION

We provide evidence for a critical role for PIP_2 as a regulator of spermatid cyst polarization during spermio-

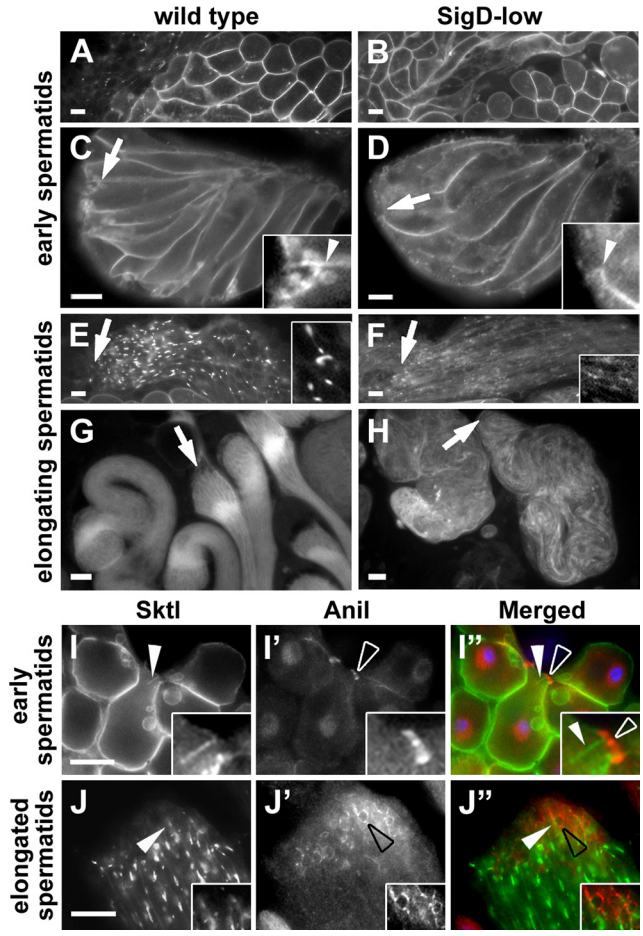

Figure 5. Sktl localizes to the growing end of spermatid cysts. (A–H) Epifluorescence micrographs showing distribution of YFP-Sktl in wild type (A, C, E, and G) and SigD-low (B, D, F, and H). Arrows indicate the growing ends of spermatid cysts. In wild-type early round spermatids (A), Sktl is evenly distributed along the plasma membrane (also shown in I). In wild-type early elongating spermatids (C), Sktl localizes along the plasma membrane and at the growing end (arrow and inset). In wild-type spermatids at midstages of elongation (E), Sktl is enriched in few focal spots along the length of the spermatid membrane and is concentrated at the growing end (inset; also shown in J). In wild-type late elongated cysts (G), Sktl is concentrated near the growing end. In early SigD-low cysts (B), Sktl localization at the plasma membrane appears normal. In contrast, in elongating SigD-low cysts (D, F, and H), Sktl fails to strongly concentrate at the growing end. (I–J″) Epifluorescence micrographs showing localization of YFP-Sktl (grayscale and green), anillin in the ring canals (Anil, red) and DNA (blue) in wild-type spermatids. During early stages of elongation (I′–I″), Sktl is found all along the plasma membrane and on the flagellar membrane (I′ and I″; insets in I and I″, white arrowheads), which is located near the ring canals (I′ and I″; insets in I′ and I″; white open arrowheads). Note that the ring canals in this cell are viewed end-on and appear as linear rather than circular structures. In later stages (J–J″), anillin remains in ring canals at the growing end (J′ and J″; black open arrowheads; insets in J′ and J″), whereas Sktl is enriched in regions adjacent to ring canals (J′ and J″; white arrowheads; insets in J and J″). Scale bars, 10 μm.

genesis. Reduction of PIP_2 levels by ectopic expression of the bacterial phosphoinositide phosphatase SigD or by mutation of the PIP5K Sktl resulted in formation of bipolar spermatid cysts. These cysts lack plasma membranes separating the elongating sperm tails, suggesting an additional defect in membrane addition during elongation. The observed effects on cyst polarity are likely due to reduction of PIP_2 or to an imbalance between PIP_2 and PI4P because studies examining genetic interactions between SigD-low and two PI4Ks as well as a PI4P phosphatase indicate that elevated levels of PI4P are not responsible for the polarity defects observed in SigD-low cysts (unpublished observations).

Our results suggest that PIP_2 localization in developing sperm primarily results from asymmetric distribution of the PIP5K Sktl rather than from localized action of the PIP_3 phosphatase PTEN (phosphatase and tensin homolog), as germ cell clones homozygous for a mutation in *PTEN* have normal polarity (unpublished observations). Subcellular localization of PIP5Ks likely represents a conserved mechanism for ensuring local synthesis of PIP_2. Localized distribution of PIP5Ks has recently been implicated in establishing cell polarity in early *Caenorhabditis elegans* embryos, as well as in root hair and pollen tube elongation in plants (Panbianco *et al.*, 2008; Sousa *et al.*, 2008; Stenzel *et al.*, 2008).

The factors that regulate localization of PIP5Ks are not well understood. In *C. elegans*, concentration of the Sktl homolog PPK-1 at the posterior pole of early embryos is dependent on casein kinase 1, which negatively regulates its distribution. In mammalian tissue culture cells, plasma membrane association of PIP5KIα is regulated by Rho and Rac (Chatah and Abrams, 2001). In neurons, mammalian PIP5KIγ661 is recruited and activated by binding to the focal adhesion protein talin and the clathrin adaptor AP-2 (Di Paolo *et al.*, 2002; Nakano-Kobayashi *et al.*, 2007). Our finding that Sktl localization is abnormal in SigD-low cysts suggests the existence of a positive feedback loop, whereby locally high concentrations of PIP_2 retain the PIP5K, which in turn stimulates local PIP_2 synthesis. Such a feedback loop could operate by maintaining locally activated Rho family G proteins, which—together with their activators—bind PIP_2 (Heo *et al.*, 2006; Yeung *et al.*, 2008; Yoshida *et al.*, 2009) and which in turn could recruit PIP5K (Yang *et al.*, 2004). Alternatively, the feedback mechanism could be more direct, because PIP5Ks were recently shown to localize to the plasma membrane via positively charged amino acids that bind phosphoinositides (Arioka *et al.*, 2004; Fairn *et al.*, 2009). In either case, mislocalization of YFP-Sktl in SigD-low cysts likely reflects a failure to retain sufficiently high levels of PIP_2 at the plasma membrane in the presence of SigD. The mechanism by which Sktl concentrates at the growing ends of spermatid cysts remains an area for future study.

We show for the first time that PIP_2 levels affect polarized exocyst distribution in a developmental context. In a survey of proteins that were candidates to be regulated by PIP_2 during spermatid cyst polarization, we discovered that actin cytoskeletal proteins (anillin, P-moesin, and spectrin) associate with the growing ends of the flagellar axonemes in the middle of the bipolar SigD-low cysts. These cytoskeletal proteins do not seem to be involved in establishing or maintaining spermatid polarity in *Drosophila*. For example, anillin is dispensable for spermatid cyst polarity (Goldbach *et al*., 2010), and PIP_2 binding by β-spectrin is not required for viability or male fertility (Das *et al.*, 2008). In contrast, the exocyst was completely delocalized upon PIP_2 reduction, and exocyst mutants show defects in spermatid cyst polarity.

Based on previous studies from yeast and mammalian cells, regulation of the exocyst by PIP_2 is likely to be direct.

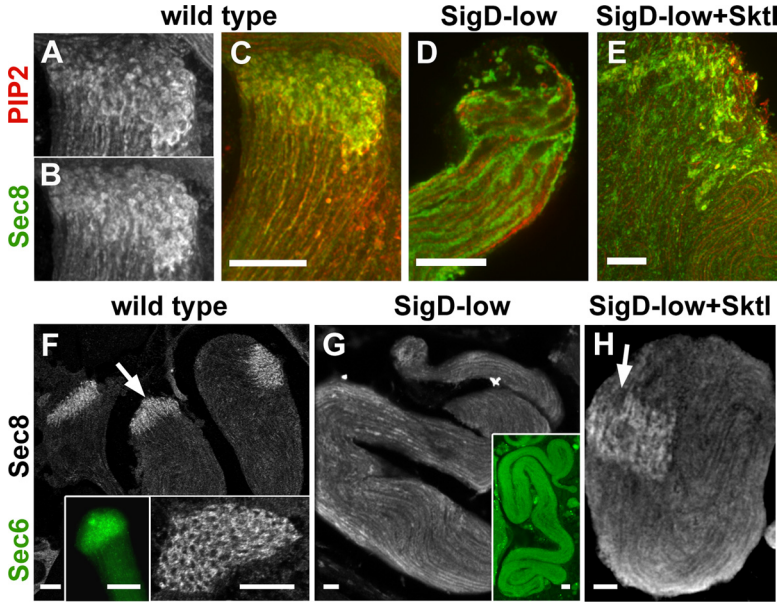

Figure 6. PIP$_2$ is required for exocyst localization at the growing end of spermatid cysts. (A–E) Confocal micrographs showing colocalization of PIP$_2$ and Sec8 by immunofluorescence. In wild type, PIP$_2$ (A) and Sec8 (B) are enriched at the growing end, with PIP$_2$ surrounding Sec8 (C). In SigD-low cysts, Sec8 fails to concentrate at the growing end (D). Coexpression of Sktl with SigD-low partially restores association of Sec8 with PIP$_2$ at the growing end (E). (F–H) Confocal micrographs showing the distribution of Sec8 (grayscale) and Sec6 (green) in elongating spermatid cysts from wild type (F), SigD-low (G), and SigD-low coexpressing Sktl (H). Arrows indicate the growing ends. In wild type, Sec8 and Sec6 localize in a honeycomb pattern at the growing end (F). Sec8 and Sec6 are delocalized in SigD-low cysts (G). Sec8 localization is partially restored by coexpression of Sktl with SigD-low (H). Scale bars, 10 μm.

Indeed, binding of the exocyst subunits Sec3 and Exo70 to PIP$_2$ appears critical for exocyst function (He *et al.*, 2007; Liu *et al.*, 2007; Zhang *et al.*, 2008). Consistent with this idea, we found that the exocyst subunit Sec8 localizes immediately adjacent to PIP$_2$ at the growing end of spermatid cysts and that localization of Sec8 and Sec6 is strongly influenced by PIP$_2$ levels: reduction of PIP$_2$ caused complete delocalization of the exocyst, and rescue of PIP$_2$ by Sktl expression restored colocalization. Furthermore, the exocyst is required for polarity of *Drosophila* spermatid cysts. A hypomorphic mutation in *fun*, which encodes Sec8, caused defects in cyst polarity, whereas loss of function of *onr*, which encodes Exo84, caused formation of apolar cysts. These defects in polarity, common to exocyst mutants and SigD transgenic flies, were not due to failure of cytokinesis, because cytokinesis was normal in SigD-low flies. Instead, our data suggest that establishment of spermatid cyst polarity relies on localized recruitment of the exocyst, which drives targeted membrane delivery to the growing end. Alternatively, or in addition, PIP$_2$ and the exocyst may help establish the axis of polarization by linking the spermatid nuclear envelope to the plasma membrane, as suggested from analysis of *sktl*$^{2-3}$ mutant clones during oogenesis (Gervais *et al.*, 2008) or by regulating formation of the flagellar membrane that surrounds the growing end of the axoneme (Fritz-Niggli and Suda, 1972; Tokuyasu, 1975). Indeed, given the structural similarity between flagella and cilia and the requirement for the exocyst in ciliogenesis, PIP$_2$ could play a conserved role in regulating this critical process.

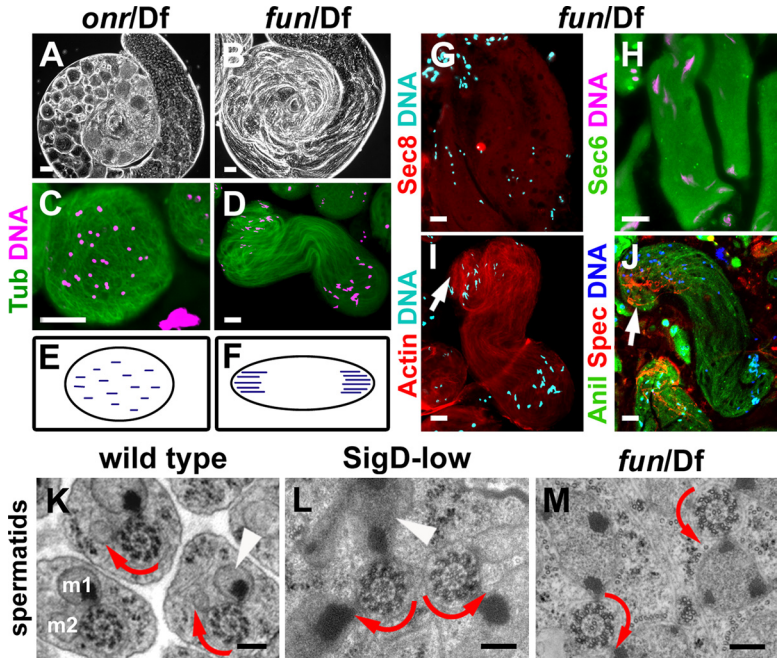

Figure 7. The exocyst and PIP$_2$ are required for spermatid elongation, polarity, and membrane addition. (A and B) Phase-contrast micrographs of whole testes, and (C and D) epifluorescence micrographs of spermatid cysts expressing β2-tubulin GFP (green) and stained for DNA (magenta). *onr* mutant cysts fail to elongate and are apolar (A and C). *fun* mutant cysts elongate and are bipolar (B and D). (E and F) Diagrams illustrating the distribution of nuclei in *onr* (E) and *fun* (F) mutant cysts. (G–J) Epifluorescence micrographs showing distribution of Sec8 (red, G), Sec6 (green, H), F-actin (red, I), α-spectrin (red, J), and anillin (green, J) relative to DNA (blue, magenta, or cyan) in *fun* mutant cysts. Arrows, the growing end (I and J). (K–M) Transmission electron micrographs showing ultrastructure of axonemes, mitochondrial derivatives and plasma membranes in early spermatids. Curved red arrows indicate rotational polarity of axonemes. White arrowheads, mitochondrial derivatives filling with electron-dense paracrystalline material. In wild-type cysts (K), axonemes show the same rotational polarity, and each axoneme is associated with a major (m1) and a minor (m2) mitochondrial derivative. In SigD-low (L) and *fun* (M) cysts, axonemes are antiparallel. Mitochondrial derivatives in SigD-low (L) and *fun* (M) contain multiple sites of filling with paracrystalline material. Scale bars (A and B), 50 μm; (C, D, and G–J), 20 μm; (K–M), 200 nm.

ACKNOWLEDGMENTS

We thank Rebecca Farkas for her initial characterization of the exocyst mutants; Christopher Bazinet, John Brumell, Kathryn Miller, and members of the Brill lab for helpful discussions; Ronit Wilk for assistance with drawings; Clare Whitehead for assistance with measuring spermatid cysts; John Ashkenas, John Brumell, Dorothea Godt, Sevan Hopyan, Helen McNeill, Julie Tan, and Ronit Wilk for critical comments on the manuscript; Yasuko Akiyama-Oda, Hiroki Oda, James Baker, Maurice Kernan, and the Bloomington *Drosophila* Stock Center for fly stocks; John Brumell, Christine Field, Brett Finlay, Slobodon Beronja, Ulrich Tepass, Sebastien Carreno, Thomas Kaufman, and the Developmental Studies Hybridoma Bank for antibodies; Paul Paroutis and Michael Woodside for help with confocal microscopy; and Robert Temkin and Yew-Meng Heng for technical assistance with electron microscopy. We are grateful for funding from a Natural Sciences and Engineering Research Council fellowship and the SickKids Restracomp program (L.F.); an American Society for Cell Biology M.A.C. award (J.R.); National Institutes of Health Grant 2R01GM062276 (M.T.F.), and a Canadian Institutes of Health Research operating grant (MOP 81336; J.A.B.).

REFERENCES

Arioka, M., Nakashima, S., Shibasaki, Y., and Kitamoto, K. (2004). Dibasic amino acid residues at the carboxy-terminal end of kinase homology domain participate in the plasma membrane localization and function of phosphatidylinositol 5-kinase gamma. Biochem. Biophys. Res. Commun. *319*, 456–463.

Baker, J. D., Adhikarakunnathu, S., and Kernan, M. J. (2004). Mechanosensory-defective, male-sterile unc mutants identify a novel basal body protein required for ciliogenesis in *Drosophila*. Development *131*, 3411–3422.

Balla, T. (2006). Phosphoinositide-derived messengers in endocrine signaling. J. Endocrinol. *188*, 135–153.

Bazinet, C., and Rollins, J. E. (2003). *Rickettsia*-like mitochondrial motility in *Drosophila* spermiogenesis. Evol. Dev. *5*, 379–385.

Behnia, R., and Munro, S. (2005). Organelle identity and the signposts for membrane traffic. Nature *438*, 597–604.

Beronja, S., Laprise, P., Papoulas, O., Pellikka, M., Sisson, J., and Tepass, U. (2005). Essential function of *Drosophila* Sec6 in apical exocytosis of epithelial photoreceptor cells. J. Cell Biol. *169*, 635–646.

Blankenship, J. T., Fuller, M. T., and Zallen, J. A. (2007). The *Drosophila* homolog of the Exo84 exocyst subunit promotes apical epithelial identity. J. Cell Sci. *120*, 3099–3110.

Carreno, S., Kouranti, I., Glusman, E. S., Fuller, M. T., Echard, A., and Payre, F. (2008). Moesin and its activating kinase Slik are required for cortical stability and microtubule organization in mitotic cells. J. Cell Biol. *180*, 739–746.

Casal, J., Gonzalez, C., and Ripoll, P. (1990). Spindles and centrosomes during male meiosis in *Drosophila melanogaster*. Eur. J. Cell Biol. *51*, 38–44.

Chatah, N. E., and Abrams, C. S. (2001). G-protein-coupled receptor activation induces the membrane translocation and activation of phosphatidylinositol-4-phosphate 5-kinase Iα by a Rac- and Rho-dependent pathway. J. Biol. Chem. *276*, 34059–34065.

Das, A., Base, C., Manna, D., Cho, W., and Dubreuil, R. R. (2008). Unexpected complexity in the mechanisms that target assembly of the spectrin cytoskeleton. J. Biol. Chem. *283*, 12643–12653.

De Matteis, M. A., and Godi, A. (2004). PI-loting membrane traffic. Nat. Cell Biol. *6*, 487–492.

Di Paolo, G., and De Camilli, P. (2006). Phosphoinositides in cell regulation and membrane dynamics. Nature *443*, 651–657.

Di Paolo, G., Pellegrini, L., Letinic, K., Cestra, G., Zoncu, R., Voronov, S., Chang, S., Guo, J., Wenk, M. R., and De Camilli, P. (2002). Recruitment and regulation of phosphatidylinositol phosphate kinase type 1 gamma by the FERM domain of talin. Nature *420*, 85–89.

Dowler, S., Currie, R. A., Campbell, D. G., Deak, M., Kular, G., Downes, C. P., and Alessi, D. R. (2000). Identification of pleckstrin-homology-domain-containing proteins with novel phosphoinositide-binding specificities. Biochem. J. *351*, 19–31.

Fairn, G. D., Ogata, K., Botelho, R. J., Stahl, P. D., Anderson, R. A., De Camilli, P., Meyer, T., Wodak, S., and Grinstein, S. (2009). An electrostatic switch displaces phosphatidylinositol phosphate kinases from the membrane during phagocytosis. J. Cell Biol. *187*, 701–714.

Field, C. M., and Alberts, B. M. (1995). Anillin, a contractile ring protein that cycles from the nucleus to the cell cortex. J. Cell Biol. *131*, 165–178.

Fritz-Niggli, H., and Suda, T. (1972). Formation and significance of centrioles: a study and new interpretation of the meiosis of *Drosophila*. Cytobiologie *5*, 12–41.

Gervais, L., Claret, S., Januschke, J., Roth, S., and Guichet, A. (2008). PIP5K-dependent production of PIP_2 sustains microtubule organization to establish polarized transport in the *Drosophila* oocyte. Development *135*, 3829–3838.

Ghosh-Roy, A., Kulkarni, M., Kumar, V., Shirolikar, S., and Ray, K. (2004). Cytoplasmic dynein-dynactin complex is required for spermatid growth but not axoneme assembly in *Drosophila*. Mol. Biol. Cell *15*, 2470–2483.

Giansanti, M. G., Farkas, R. M., Bonaccorsi, S., Lindsley, D. L., Wakimoto, B. T., Fuller, M. T., and Gatti, M. (2004). Genetic dissection of meiotic cytokinesis in *Drosophila* males. Mol. Biol. Cell *15*, 2509–2522.

Goldbach, P., Wong, R., Beise, N., Sarpal, R., Trimble, W. S., and Brill, J. A. (2010). Stabilization of the Actomyosin Ring Enables Spermatocyte Cytokinesis in *Drosophila*. Mol. Biol. Cell *21*, 1482–1493.

Golic, K. G., and Lindquist, S. (1989). The FLP recombinase of yeast catalyzes site-specific recombination in the *Drosophila* genome. Cell *59*, 499–509.

Hala, M., *et al.* (2008). An exocyst complex functions in plant cell growth in *Arabidopsis* and tobacco. Plant Cell *20*, 1330–1345.

He, B., Xi, F., Zhang, X., Zhang, J., and Guo, W. (2007). Exo70 interacts with phospholipids and mediates the targeting of the exocyst to the plasma membrane. EMBO J. *26*, 4053–4065.

Hense, W., Baines, J. F., and Parsch, J. (2007). X chromosome inactivation during *Drosophila* spermatogenesis. PLoS Biol. *5*, e273.

Heo, W. D., Inoue, T., Park, W. S., Kim, M. L., Park, B. O., Wandless, T. J., and Meyer, T. (2006). $PI(3,4,5)P_3$ and $PI(4,5)P_2$ lipids target proteins with polybasic clusters to the plasma membrane. Science *314*, 1458–1461.

Hime, G. R., Brill, J. A., and Fuller, M. T. (1996). Assembly of ring canals in the male germ line from structural components of the contractile ring. J. Cell Sci. *109*, 2779–2788.

Hirao, M., Sato, N., Kondo, T., Yonemura, S., Monden, M., Sasaki, T., Takai, Y., and Tsukita, S. (1996). Regulation mechanism of ERM (ezrin/radixin/moesin) protein/plasma membrane association: possible involvement of phosphatidylinositol turnover and Rho-dependent signaling pathway. J. Cell Biol. *135*, 37–51.

Hoyle, H. D., and Raff, E. C. (1990). Two *Drosophila* beta tubulin isoforms are not functionally equivalent. J. Cell Biol. *111*, 1009–1026.

Hsu, S. C., TerBush, D., Abraham, M., and Guo, W. (2004). The exocyst complex in polarized exocytosis. Int. Rev. Cytol. *233*, 243–265.

Inoue, Y. H., Savoian, M. S., Suzuki, T., Mathe, E., Yamamoto, M. T., and Glover, D. M. (2004). Mutations in *orbit/mast* reveal that the central spindle is comprised of two microtubule populations, those that initiate cleavage and those that propagate furrow ingression. J. Cell Biol. *166*, 49–60.

Lemmon, M. A., Ferguson, K. M., O'Brien, R., Sigler, P. B., and Schlessinger, J. (1995). Specific and high-affinity binding of inositol phosphates to an isolated pleckstrin homology domain. Proc. Natl. Acad. Sci. USA *92*, 10472–10476.

Li, K., Xu, E. Y., Cecil, J. K., Turner, F. R., Megraw, T. L., and Kaufman, T. C. (1998). *Drosophila* centrosomin protein is required for male meiosis and assembly of the flagellar axoneme. J. Cell Biol. *141*, 455–467.

Liu, J., Zuo, X., Yue, P., and Guo, W. (2007). Phosphatidylinositol 4,5-bisphosphate mediates the targeting of the exocyst to the plasma membrane for exocytosis in mammalian cells. Mol. Biol. Cell *18*, 4483–4492.

Nakano-Kobayashi, A., Yamazaki, M., Unoki, T., Hongu, T., Murata, C., Taguchi, R., Katada, T., Frohman, M. A., Yokozeki, T., and Kanaho, Y. (2007). Role of activation of PIP5Kγ661 by AP-2 complex in synaptic vesicle endocytosis. EMBO J. *26*, 1105–1116.

Niggli, V. (2005). Regulation of protein activities by phosphoinositide phosphates. Annu. Rev. Cell Dev. Biol. *21*, 57–79.

Niggli, V., Andreoli, C., Roy, C., and Mangeat, P. (1995). Identification of a phosphatidylinositol-4,5-bisphosphate-binding domain in the N-terminal region of ezrin. FEBS Lett. *376*, 172–176.

Noguchi, T., and Miller, K. G. (2003). A role for actin dynamics in individualization during spermatogenesis in *Drosophila melanogaster*. Development *130*, 1805–1816.

Odorizzi, G., Babst, M., and Emr, S. D. (2000). Phosphoinositide signaling and the regulation of membrane trafficking in yeast. Trends Biochem. Sci. *25*, 229–235.

Oude Weernink, P. A., Lopez de Jesus, M., and Schmidt, M. (2007). Phospholipase D signaling: orchestration by PIP_2 and small GTPases. Naunyn Schmiedebergs Arch. Pharmacol. *374*, 399–411.

Panbianco, C., Weinkove, D., Zanin, E., Jones, D., Divecha, N., Gotta, M., and Ahringer, J. (2008). A casein kinase 1 and PAR proteins regulate asymmetry of a PIP_2 synthesis enzyme for asymmetric spindle positioning. Dev. Cell *15*, 198–208.

Peters, P. J., Bos, E., and Griekspoor, A. (2006). Cryo-immunogold electron microscopy. In: Current Protocols in Cell Biology, ed. J. Bonifacino, M. Dasso, J. Harford, J. Lippincott-Schwartz, and K. Yamada, New York: Wiley, 4.7.1–4.7.19.

Roth, M. G. (2004). Phosphoinositides in constitutive membrane traffic. Physiol. Rev. *84*, 699–730.

Sambrook, J., Fritsch, E. F., and Maniatis, T. (1989). Molecular Cloning: A Laboratory Manual, Cold Spring Harbor, NY: Cold Spring Harbor Press.

Somers, W. G., and Chia, W. (2005). Recycling polarity. Dev. Cell *9*, 312–313.

Sousa, E., Kost, B., and Malho, R. (2008). *Arabidopsis* phosphatidylinositol-4-monophosphate 5-kinase 4 regulates pollen tube growth and polarity by modulating membrane recycling. Plant Cell *20*, 3050–3064.

Stenzel, I., Ischebeck, T., Konig, S., Holubowska, A., Sporysz, M., Hause, B., and Heilmann, I. (2008). The type B phosphatidylinositol-4-phosphate 5-kinase 3 is essential for root hair formation in *Arabidopsis thaliana.* Plant Cell *20*, 124–141.

Takenawa, T., and Itoh, T. (2001). Phosphoinositides, key molecules for regulation of actin cytoskeletal organization and membrane traffic from the plasma membrane. Biochim. Biophys. Acta *1533*, 190–206.

Tates, A. D. (1971). Cytodifferentiation during spermatogenesis in *Drosophila melanogaster*: an electron microscope study. Ph. D. dissertation. Leiden: Rijksuniversiteit.

Tokuyasu, K. T. (1975). Dynamics of spermiogenesis in *Drosophila melanogaster*. VI. Significance of "onion" nebenkern formation. J. Ultrastruct. Res. *53*, 93–112.

Varnai, P., and Balla, T. (1998). Visualization of phosphoinositides that bind pleckstrin homology domains: calcium- and agonist-induced dynamic changes and relationship to myo-[^{3}H]inositol-labeled phosphoinositide pools. J. Cell Biol. *143*, 501–510.

Wakimoto, B. T., Lindsley, D. L., and Herrera, C. (2004). Toward a comprehensive genetic analysis of male fertility in *Drosophila melanogaster*. Genetics *167*, 207–216.

Wei, H. C., Rollins, J., Fabian, L., Hayes, M., Polevoy, G., Bazinet, C., and Brill, J. A. (2008). Depletion of plasma membrane PtdIns(4,5)P_2 reveals essential roles for phosphoinositides in flagellar biogenesis. J. Cell Sci. *121*, 1076–1084.

Wong, R., Hadjiyanni, I., Wei, H. C., Polevoy, G., McBride, R., Sem, K. P., and Brill, J. A. (2005). PIP_2 hydrolysis and calcium release are required for cytokinesis in *Drosophila* spermatocytes. Curr. Biol. *15*, 1401–1406.

Yamashita, M., Kurokawa, K., Sato, Y., Yamagata, A., Mimura, H., Yoshikawa, A., Sato, K., Nakano, A., and Fukai, S. (2010). Structural basis for the Rho- and phosphoinositide-dependent localization of the exocyst subunit Sec3. Nat. Struct. Mol. Biol. *17*, 180–186.

Yang, S. A., Carpenter, C. L., and Abrams, C. S. (2004). Rho and Rho-kinase mediate thrombin-induced phosphatidylinositol 4-phosphate 5-kinase trafficking in platelets. J. Biol. Chem. *279*, 42331–42336.

Yeung, T., Gilbert, G. E., Shi, J., Silvius, J., Kapus, A., and Grinstein, S. (2008). Membrane phosphatidylserine regulates surface charge and protein localization. Science *319*, 210–213.

Yin, H. L., and Janmey, P. A. (2003). Phosphoinositide regulation of the actin cytoskeleton. Annu. Rev. Physiol. *65*, 761–789.

Yoshida, S., Bartolini, S., and Pellman, D. (2009). Mechanisms for concentrating Rho1 during cytokinesis. Genes Dev. *23*, 810–823.

Zhang, X., Orlando, K., He, B., Xi, F., Zhang, J., Zajac, A., and Guo, W. (2008). Membrane association and functional regulation of Sec3 by phospholipids and Cdc42. J. Cell Biol. *180*, 145–158.

Zuo, X., Guo, W., and Lipschutz, J. H. (2009). The exocyst protein Sec10 is necessary for primary ciliogenesis and cystogenesis *in vitro*. Mol. Biol. Cell *20*, 2522–2529.